Available online at www.sciencedirect.com
SCIENCE DIRECT®
PERGAMON
International Journal of Heat and Mass Transfer 46 (2003) 3189–3199
International Journal of HEAT and MASS TRANSFER
www.elsevier.com/locate/ijhmt

Unsteady flow and heat transfer in plane channels with spatially periodic vortex generators

Alvaro Valencia [a,*], Mihir Sen [b]

[a] Department of Mechanical Engineering, Universidad de Chile, Casilla 2777, Santiago, Chile
[b] Department of Aerospace and Mechanical Engineering, University of Notre Dame, Notre Dame, IN 46556, USA

Received 25 October 2002; received in revised form 4 February 2003

Abstract

The flow structure and heat transfer in a plane channel with periodically placed vortex generators of different forms have been investigated in the Reynolds number range corresponding to unsteady laminar and transitional flow. Numerical results from four different configurations are reported: a pair of square bars, a rectangular bar, and two different baffle arrangements. The heat transfer and pressure drop are strongly dependent on the geometry used. A wide range of geometric parameters have been computed to cover the different possibilities. The unsteady Navier–Stokes equations and the energy equation have been solved by a finite-volume code with staggered grids combined with SIMPLEC pressure correction. The velocity and temperature fields were computed. Results for the same pumping power show heat transfer enhancement by a factor larger than 3.5 in the best cases.

1. Introduction

The flow between fins in compact heat exchangers is often through spaces with small hydraulic diameters and is consequently at small Reynolds numbers, *Re*, in the 100–1000 range for which the flow is laminar. Since it is desired to have the highest possible heat transfer between the fin and the fluid, these devices frequently employ surfaces for heat transfer enhancement by geometric means [1]. Fins are typically used to extend surface areas while enhancement techniques depend more on modification of the flow. For example, offset strips can be used to decrease the thickness of the thermal boundary layers, or transversely grooved channels and passages can be used to excite normally damped Tollmien–Schlichting waves [2,3]. Another possible technique is to create vortices to augment fluid mixing. Two main vortex orientations can be distinguished: transverse vortices which have their axes transverse to the flow and lead to two-dimensional flow, and longitudinal vortices which have their axes along the flow in the streamwise direction with consequent three-dimensionality [4]. In this work we will study the former orientation.

Investigations have been made on the generation of vortices and their influence on flow structure and heat transfer for fully developed channel flows. Longitudinal vortex generators in the form of winglets on the channel surface and transverse ones in the form of baffles have been analyzed. Numerical computations have played a key role in our understanding of the phenomena. For computational purposes spatially periodic generators with periodic boundary conditions are generally used. The results of numerical and experimental investigations for a transverse generator in a plane channel of separation H with one spatially periodic baffle of height $0.5H$ on the channel wall and with a longitudinal pitch of $P = 5H$ showed that self-sustained oscillations were present at $Re = 93$. Heat transfer enhancement was found only with unsteady flow [5].

Roberts [6] reported numerical and experimental results of the flow transition processes in a channel with in-line baffles. At a critical *Re* of approximately 100 the flow became asymmetric and unsteady. This led to an eddy shedding regime with eddies formed and shed successively from each baffle. Wang et al. [7] investigated

* Corresponding author. Tel.: +56-2-6784386; fax: +56-2-6988453.
E-mail address: alvalenc@cec.uchile.cl (A. Valencia).

0017-9310/03/$ - see front matter © 2003 Elsevier Science Ltd. All rights reserved.
doi:10.1016/S0017-9310(03)00099-1

Nomenclature

C_{d1}	drag coefficient on bottom bar
C_{d2}	drag coefficient on top bar
C_{l1}	lift coefficient on bottom bar
C_{l2}	lift coefficient on top bar
d	bar height, m
e	baffle thickness, m
f	friction factor
F	eddy shedding frequency, s^{-1}
H	channel height, m
L	longitudinal bar separation distance, m
Nu	mean Nusselt number
P	spatial pitch, m
Pr	Prandtl number $= v/\alpha$
Re	channel Reynolds number $= \overline{u}H/v$
S	Strouhal number $= Fd/\overline{u}$
T	transverse bar separation distance, m
T_0	reference temperature, K
$\overline{u}$	channel-averaged velocity at inlet, $m\,s^{-1}$
U_{max}	maximum non-dimensional velocity component
X	non-dimensional Cartesian coordinate
ΔX	spatial discretization step
Greek symbols	
α	thermal diffusivity, $m^2\,s^{-1}$
v	fluid kinematic viscosity
ρ	fluid density
$\Delta\tau$	computational time step

the enhancement of heat transfer due to unsteady flow in channels with in-line and staggered baffles for which the flow becomes naturally unsteady at Re around 110 and 200, respectively. They used baffle heights of $0.25H$ and a pitch of $1.5H$. Significant increases in heat transfer rates were reported once the flow became unsteady, and the heat transfer enhancements were nearly the same in both configurations. Kozlu et al. [8] showed that the periodic addition of cylinders in a plane channel near the wall can significantly reduce the value of Re for laminar to turbulent transition. Heat transfer on the heated channel wall and the friction coefficient increase due to flow instability induced by the cylinders.

Valencia [9] studied unsteady flow and heat transfer in plane channels with periodically placed rectangular bars of height $0.5H$ on the channel axis and quantified the benefits of self-sustained oscillations for pitches of $2.25H$, $4.25H$ and $6.25H$. Calculations were performed for $Re = 100$–400 ranging from steady laminar to transitional flows. A comparison of the mean Nusselt number, Nu, as a function of the pumping power for the three configurations shows that for the same pumping power the heat transfer is largest with the pitch $2.25H$. Valencia et al. [10] employed numerical simulations to explore the fluid flow and heat transfer in channels with two side by side square bars of size $0.2H$. Computations were made for separation distances between the bars T/d of 1.5, 2, 2.5 and 3, where T is the separation and d is the bar height, with $Re = 300$ and a pitch of $2H$. The numerical results reveal the complex structure of the unsteady flow. As a consequence of vortex shedding around the bars, there is significant heat transfer enhancement on the channel walls. The interaction of flow between the bars and the flow between them and the channel walls considerably affects the performance of these geometries.

Bosch [11] categorized the flow pattern for a pair of square bars in a side by side arrangement into three regimes: single vortex street, bistable flow, and double vortex streets. For transverse bar separation distances of $T/d \leqslant 1.4$, a single vortex street is formed as for a single bluff body. For $1.4 \leqslant T/d \leqslant 2.4$, the flow is biased to one side and intermittently flips to the other. The flow changes from the biased pattern to two symmetric vortex streets for $T/d \geqslant 2.4$ and either in-phase or out-of-phase vortices are possible. However the characteristics of the unsteady flow are not the same if periodic boundary conditions exist and the bars are in a plane channel [10].

The heat transfer and the pumping power in a plane channel with pairs of square bars that are spatially periodic depend on the bar height, the pitch, the longitudinal and transverse bar separation distances, in addition to Re and the Prandtl number, Pr. The previous papers only partially cover the influence of these parameters. In addition, it is difficult to compare the results of heat transfer enhancement between the different geometries that have been investigated due to the different computational boundary conditions used and experimental and numerical uncertainties.

The current work is a numerical investigation of heat transfer in a plane channel with pairs of square bars, with one rectangular bar, and with baffles all repeated in a spatially periodic fashion. The computations can be kept two-dimensional by restricting to Reynolds numbers lower than those for three-dimensionality as found by Breuer et al. [12]. Many different arrangements have been computed and in some of them the influence of Re has been studied in detail for air flow in the range of $175 \leqslant Re \leqslant 1000$. The objective of the present work is to quantify the effects of geometrical parameters and Re on these geometries to obtain an optimal design.

2. Mathematical formulation

The flow is assumed to be unsteady, two-dimensional and laminar. The conservation equations are the continuity, the time-dependent Navier–Stokes, and the energy equations. The fluid is assumed to be Newtonian with constant properties and the dissipation terms in the energy equation are neglected. The velocities are non-dimensionalized with the mean velocity $\overline{u}$, all lengths with the channel separation H, the pressure with $\rho\overline{u}^2$, the temperature with a reference temperature T_0, and time with $H/\overline{u}$. The channel Reynolds number is defined with respect to $\overline{u}$ and H. The Prandtl number of the fluid is taken to be $Pr = 0.71$ corresponding to air. Most of the variables will be non-dimensional from now on.

Spatial periodicity of the solution will be assumed and therefore the computation will be limited to one basic unit. Implicit is the assumption that the flow is fully developed, both hydrodynamically and thermally. To enable analysis of periodic boundary conditions, the pressure is written as the sum of a mean linear and a time-dependent fluctuating part [13]. The slope of the mean part is adjusted at every time step to satisfy the fixed mass flow condition. Spatially periodic boundary conditions are imposed on the velocities and on the fluctuating part of the pressure. Periodicity of the thermal boundary condition in the X-direction is also imposed. The bulk temperature is calculated and the Nusselt number Nu defined in terms of that and the instantaneous heat transfer. The instantaneous flow losses are evaluated with the friction factor f defined as the combined effect of skin friction and the drag on the vortex generators.

The vortex generators are assumed to be of a material with thermal conductivity different from that of air. The detached generators do not have an imposed temperature, while the ones attached to the walls act as fins. For numerical purposes we have considered generators of duralumin which has a thermal conductivity 6400 times that of air. The energy equation was modified in the region of the generators to consider the effect of this on the temperature field. The governing non-dimensional equations are written out in detail in [9,10] and will not be repeated here.

3. Configurations and verification

Four different arrangements were studied, as shown schematically in Fig. 1. The arrangements are repeated spatially and only one unit is shown. Each one has different geometrical parameters and their values are in Tables 1–3. The different configurations and parameter values will be referred to as cases a_i, b_i, etc. Fig. 1(a) shows two square bars; the geometrical parameters are T/d, L/d, d/H and P/H in Table 1. a_7 and a_9 are similar to [10] for $Re = 300$.

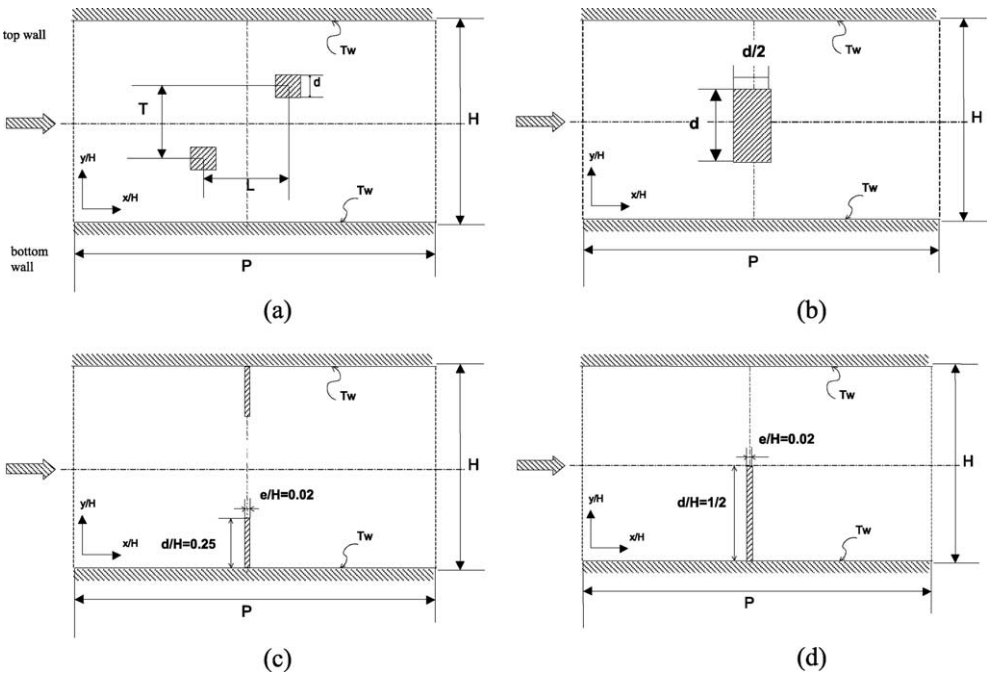

Fig. 1. Computational domain.

Table 1
Geometrical parameters for a pair of square bars (Fig. 1 (a))

Case	L/d	T/d	d/H	P/H	Re
a_1	0	1.75	0.125	2	200, 250, 300, 400, 600, 800, 1000
a_2	2	1.75	0.125	2	800
a_3	8	4	0.125	2	800
a_4	0	4	0.125	2	800
a_5	0	3	0.125	2	800
a_6	0	1.5	0.125	2	800
a_7	0	1.75	0.2	2	400
a_8	0	4	0.2	1.5	400
a_9	0	3	0.2	2	400
a_{10}	0	1.5	0.125	1	800
a_{11}	0	1.5	0.125	0.75	800

Table 2
Geometrical parameters for one rectangular bar (Fig. 1(b))

Case	d/H	P/H	Re
b_1	0.125	2	800
b_2	0.25	2	200, 400, 600, 800
b_3	0.4	2	200, 300, 400, 600
b_4	0.5	2	400
b_5	0.4	1.5	400
b_6	0.4	1	400

Table 3
Geometrical parameters for one baffle (Fig. 1(d)) and two baffles (Fig. 1(c))

Case	P/H	Re
c_1	1.5	400
d_1	1.5	400
d_2	5	100, 175

Fig. 1(b) shows one rectangular bar in the plane channel. The geometrical parameters here are d/H and P/H with the values in Table 2. b_3 and b_4 are also similar to those in [9] and [10], respectively.

Fig. 1(c) shows two baffles attached to the channel walls with the parameters shown in Table 3. This was also studied in [6,7]. We calculated this configuration for comparison, and to eliminate the differences in Nu coming from different definitions. Wang et al. [7] computed instantaneous Nu that were negative on the channel walls. With the present periodic boundary conditions this parameter is always positive. Computations with a small time step of $\Delta\tau = 0.0007$ and grid resolution of 288×192 control volumes show the same unsteady asymmetric flow as in [6]. The dominant frequency in the drag coefficient was found to be 0.125, whereas the frequency of the least stable mode was reported to be 0.117 in [6]. The friction factor was computed to be 0.632, compared to the value of 0.64 in [7].

Fig. 1(d) is a modification of Fig. 1(c) with only one baffle on the channel wall. The parameters are shown in Table 3. d_2 was studied in [5] with a grid of 80×400 control volumes and we used the same configuration for verification of our program. For d_2 we also performed computation for steady flow with $Re = 100$. Comparing with the previous results, the differences were less than 1% in Nu and 11% in skin friction coefficients. For the comparison we used a grid size of 128×640 control volumes with $\Delta\tau = 0.001$. For unsteady flow in d_2, the Strouhal number was calculated to be $S = 0.265$ compared to a previous value of 0.25, the heat transfer enhancement was 1.79 instead of 1.8, and the pressure drop increase was 6.0 instead of 6.4.

4. Numerical method

The present study uses a control volume formulation, details of which are in [14]. Several modifications to the application of the SIMPLE method recommended in [15], including the SIMPLEC approximation, tridiagonal matrix solver and convergence criterion for the pressure correction equation, are implemented in the present algorithm. For the solution of the resulting matrices with periodic boundary conditions a special tridiagonal-matrix solver was programmed. The same governing equations are used for the vortex generators. Zero velocity on the bars is achieved by adding a source

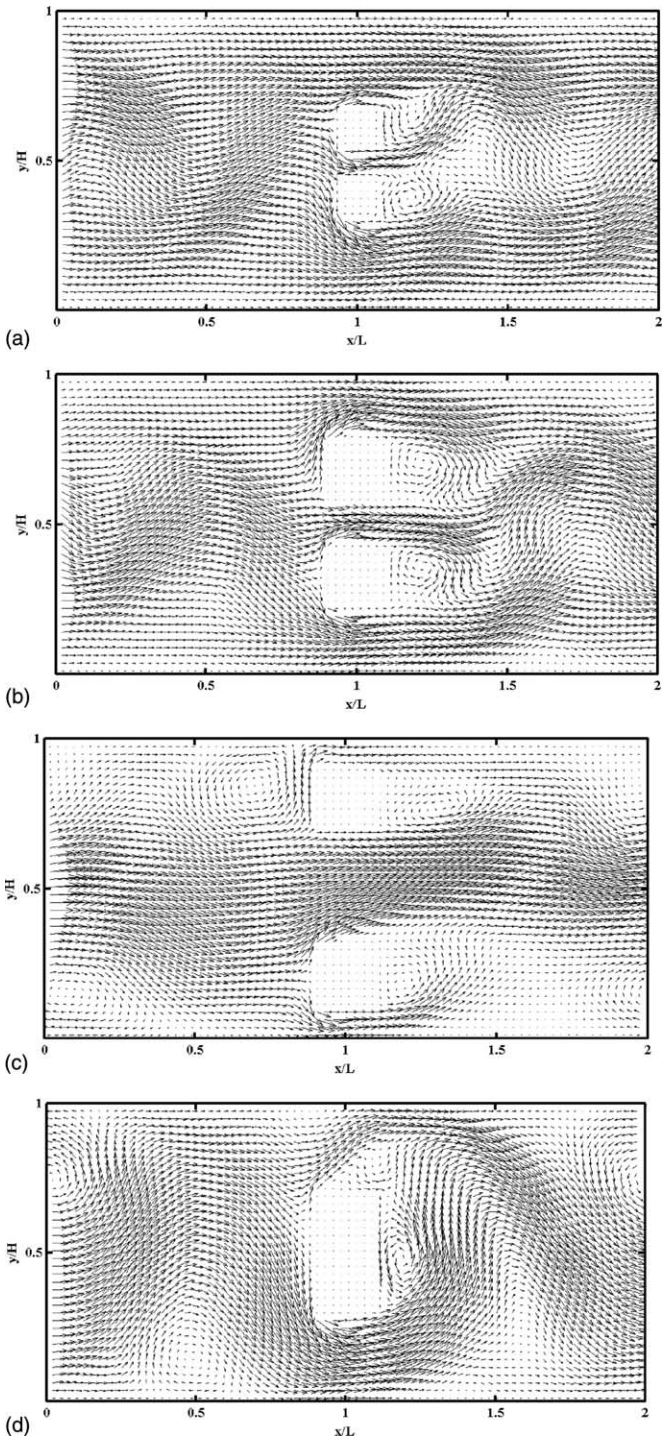

Fig. 2. Instantaneous maps of velocity vectors for $Re = 400$; (a) a_1, (b) a_7, (c) a_9, (d) b_3.

term of very high magnitude in the Navier–Stokes equations in the control volumes where the generators are located. Computations that are fully implicit and explicit in time were run for the case a_1 with $Re = 400$ and with a time step of 0.0007 and no difference was found between them, so that the explicit method was

used for the results shown. The spatial discretization is correct to second order. About 100 iterations were found to be sufficient for the SIMPLEC pressure correction procedure to converge.

To show that it is sufficient to compute one spatially periodic unit, numerical simulations with a domain containing one or two rectangular bars for b_1 were carried out. Very fine grids of 384×192 and 768×192 control volumes were used. The flow structures in the two units were anti-symmetric, the computed differences on the global *Nu*, drag coefficients, mean skin friction coefficients, and Strouhal number between the one and two period calculations were smaller than 10%.

To check grid independence, numerical simulations of the unsteady problem for a_1 were performed on grids of 352×176, 384×192, and 416×208 for $Re = 250$ and 800. In all the grid sizes an explicit time integration with a constant Courant number $U_{\max}\Delta\tau/\Delta X = 0.2$ was used. Values of integral parameters such as the mean drag coefficients, mean skin friction coefficients, mean *Nu* on the channel walls, friction factor, and eddy-shedding Strouhal number of the flow were compared. The parameter with the most difference between the three grids was the mean drag coefficient. For a simple, unsteady laminar flow with $Re = 250$ the differences were smaller than 4%. With the complex, unsteady transitional flow for $Re = 800$ the differences on the mean value of drag coefficients were lower than 9%. Therefore, we have used an intermediate grid of 192 $(P/H) \times 192$ control volumes with $\Delta\tau = 0.0007$ for all the calculations in this work. All the computations with a complex, unsteady transitional flow characterized by the presence of several dominant frequencies were calculated until a time around 100. That takes about 143,000 time steps and needs more than 7000 CPU minutes in a personal computer with a Pentium IV processor.

5. Results and discussion

The structure of the flow in the periodic regime will first be discussed. It can be illustrated through the use of the instantaneous velocity vectors. Fig. 2 shows instantaneous maps of velocity vectors for a_1, a_7, a_9 and b_3 and $Re = 400$. One can notice unsteady vortices generated in the channel due the bars, and in a_9 and b_3 vortices upstream of the bars also. The unsteady vortices mix core fluid with near-wall fluid. The Karman vortex sheets are shed from the downstream face of the bars and travel through the channel, washing across the upstream face of the next bars. Thus, the upstream face of the bars are exposed to a periodically induced flushing. For the pair of square bars the transverse separation distance between them and the bar size influence the generation of the unsteady vortices.

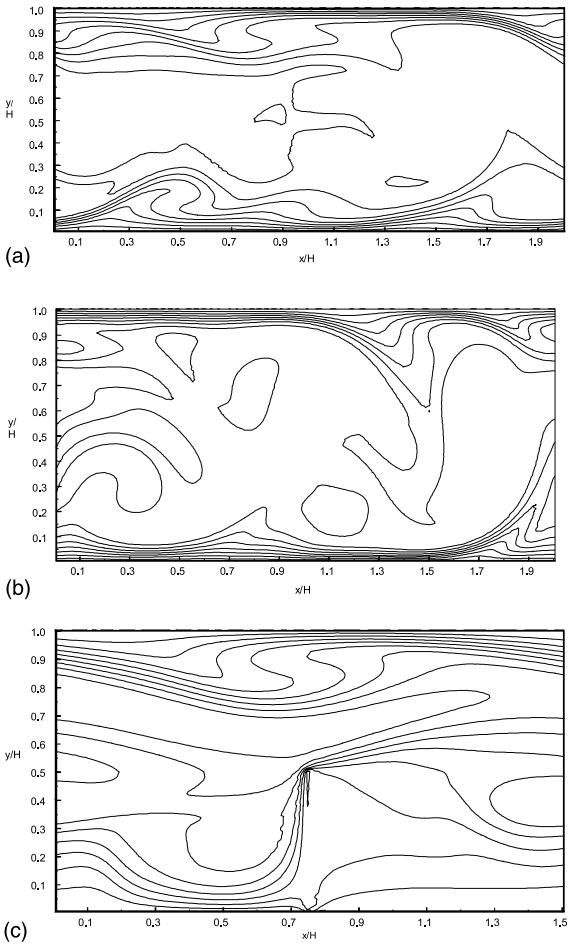

Fig. 3. Instantaneous isotherms; (a) a_1, $Re = 800$, (b) a_6, $Re = 800$, (c) d_1, $Re = 400$.

Fig. 3 shows the instantaneous isotherms for a_1 and a_6 with $Re = 800$, and d_1 with $Re = 400$. The structure of the temperature fields are a reflection of the velocities. As expected, the gradients in the temperature are largest in the near-wall region and in the shear layers. a_6 shows higher temperature gradients than for a_1 near the walls, and therefore higher local heat transfer coefficients. The fin effect in d_1 is clearly seen in Fig. 3(c).

Fig. 4 shows the power spectral density of drag coefficients for the bottom and top square bars in the channel for a_1 with $Re = 400$ and 800. The frequencies have been non-dimensionalized by H and $\bar{u}$, and therefore they do not correspond to the Strouhal number S. The signals were processed by an FFT routine. The characteristic frequency $FH/\bar{u}$ of vortex shedding around a square bar in a channel is around 1.5 in a simple, unsteady laminar flow; however, this frequency dominates only for $Re = 400$. The spectrum indicates that the flow is at the beginning of transition for $Re = 400$, and

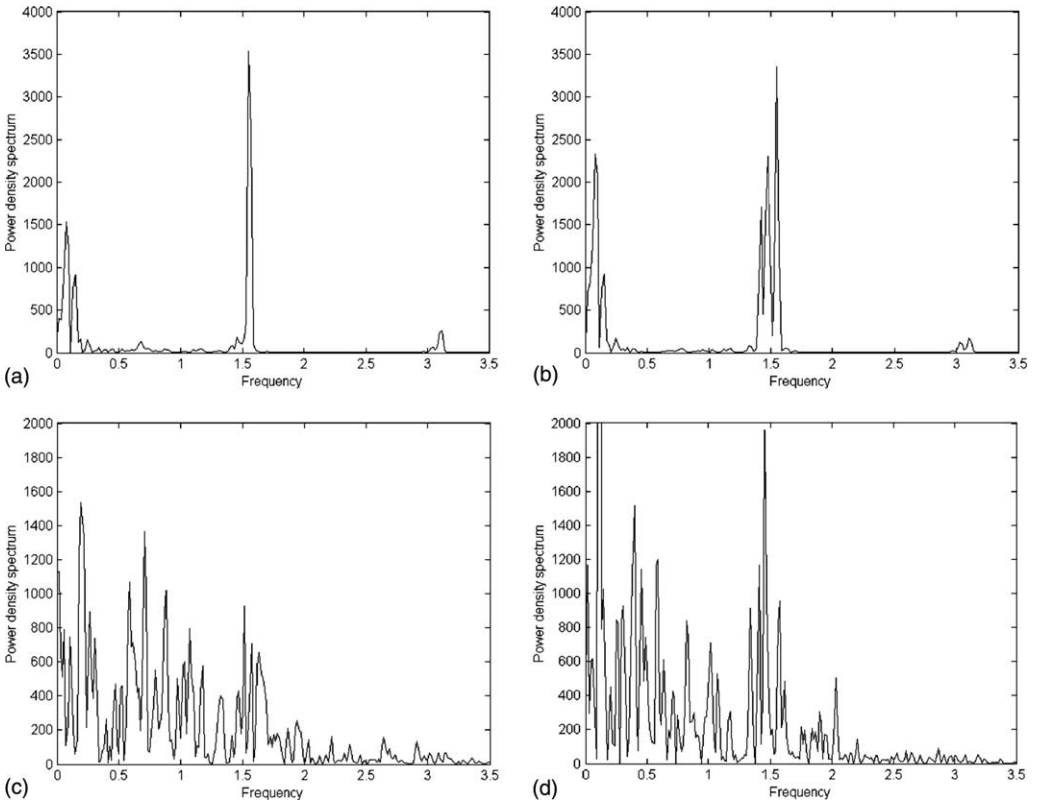

Fig. 4. Power spectral density of drag coefficients of bottom and top bars a_1; (a) bottom bar with $Re = 400$, (b) top bar with $Re = 400$, (c) bottom bar with $Re = 800$, (d) top bar with $Re = 800$.

near the end for 800. A comparison of the spectra between the two bars shows that the unsteady transitional flow around the bars is different.

Mean integral parameters of the unsteady flow around the square bars, such as the drag and lift coefficients, and eddy shedding frequencies expressed as Strouhal numbers are shown in Table 4. One can distinguish between simple, unsteady laminar flows (*sulf*) characterized with only one frequency present and complex, unsteady transitional flow (*cutf*) with several frequencies. In *sulf* the mean values around the two bars are nearly the same. In *cutf* the Strouhal numbers indicated are only three of the many dominant frequencies present in the flow, as also shown in Fig. 4. The lift coefficients in a_8 are zero, because the square bars are attached to the channel walls. In a_{11} the lift coefficients are also zero, because with the small pitch of $P/H = 0.75$ we have anti-symmetric *sulf*.

For rectangular bars we have found *sulf* modes only for b_2 with $Re = 200$ and b_3 with $Re = 200$, and in b_6. All the rest of the geometries with one built-in rectangular bar as vortex generator have *cutf* mode. The Strouhal numbers range from 0.08 to 0.9.

Figs. 5 and 6 show the influence of the unsteady vortex sheets that are shed by the square and rectangular bars on the instantaneous *Nu* on the bottom channel wall and the friction factor for a_1 and b_2 with $Re = 800$. The temporal dependence of heat transfer and pressure drop in both geometries show the effects of the presence of the *cutf* mode. In b_2 the amplitudes of the oscillations in *Nu* and friction factor are greater than for a_1.

Fig. 7 shows the mean *Nu* for all the computations and the variation with Reynolds number for three of them. The *Nu* for a laminar plane channel taken from [16] is also shown, along with one louvered plate channel taken from [17]. A comparison of a_6, a_{10} and a_{11} shows that the optimal pitch is around $P/H = 1.0$; a lower pitch produces a great reduction in *Nu*. The optimal T/d depends on d/H; it is around 1.5 for $d/H = 0.125$ and 3.0 for $d/H = 0.2$. The simple, symmetrical arrangement of the vortex generators in-line or staggered, a_4 and a_3, do not produce high *Nu*. Attached square bars on the channel walls, a_8, produces a low *Nu*. a_1 has nearly the same heat transfer as d_1 and d_2 with only one baffle. A comparison of b_3, b_5 and b_6 shows that the optimal pitch for the rectangular bar is around $P/H = 1.5$; a lower

Table 4
Mean drag coefficient, lift coefficient, and Strouhal numbers for the square bars; S is calculated from time signal of bottom bar

Case	Re	C_{d1}	C_{d2}	C_{l1}	C_{l2}	S	Flow
a_1	200	4.54	4.55	−1.67	1.64	0.14	*sulf*
	250	4.47	4.47	−1.64	1.63	0.14	*sulf*
	300	3.76	4.05	−1.39	1.15	0.01, 0.18, 0.19	*cutf*
	400	4.06	3.74	−1.06	1.36	0.01, 0.02, 0.19	*cutf*
	600	4.35	4.13	−1.06	1.37	0.08, 0.10, 0.20	*cutf*
	800	4.34	4.04	−0.96	1.24	0.02, 0.09, 0.19	*cutf*
	1000	4.09	4.13	−1.02	0.97	0.07, 0.12, 0.19	*cutf*
a_2	800	2.90	3.31	−0.51	−0.03	0.02, 0.09, 0.17	*cutf*
a_3	800	2.57	2.61	−0.29	0.30	0.05, 0.07, 0.14	*cutf*
a_4	800	2.75	2.76	−0.35	0.37	0.06, 0.15, 0.20	*cutf*
a_5	800	3.15	3.45	−0.34	0.37	0.05, 0.06, 0.21	*cutf*
a_6	800	5.58	5.44	−1.48	1.57	0.06, 0.09, 0.13	*cutf*
a_7	400	5.58	5.58	−1.63	1.61	0.32	*sulf*
a_8	400	1.02	1.07	0	0	0.12	*sulf*
a_9	400	3.96	4.06	0.16	−0.16	0.08, 0.20, 0.28	*cutf*
a_{10}	800	4.65	4.52	−0.80	0.80	0.02, 0.05, 0.13	*cutf*
a_{11}	800	0.73	0.80	0	0	0.16	*sulf*

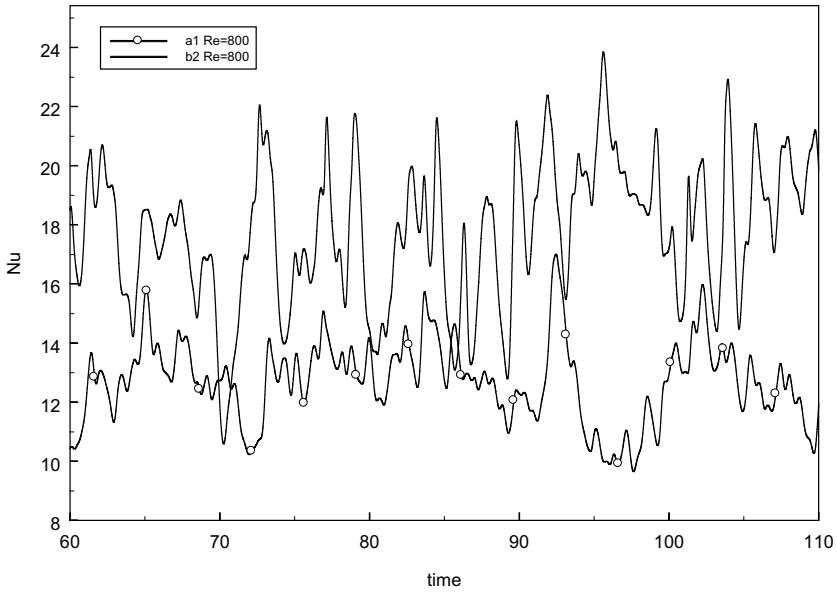

Fig. 5. Nusselt number for a_1 and b_2 with $Re = 800$ as function of time.

pitch produces again a reduction in Nu. The rectangular bar of $d/H = 0.4$ has a optimal size for heat transfer enhancement. b_2 has nearly the same Nu as a_{10} with two square bars and c_1 with two in-line baffles. For the same Re the heat transfer enhancement with built-in generators can be higher than a factor 5 compared with a plane channel, and in the most arrangements is higher than a louvered plate channel.

Fig. 8 shows the variation of friction factor with the Reynolds number. For one rectangular bar these are in general higher than with two square bars. The variation with Re is different for b_2 and b_3 compared with a_1 due the interaction of the unsteady flow around the two bars.

Fig. 9 shows a comparison of the mean Nu as a function of the pumping power. Oscillatory flows require less pumping power than turbulent flows to achieve the same transport rates, because the self-sustained oscillations yield less viscous dissipation than random chaotic turbulent fluctuations. The geometries

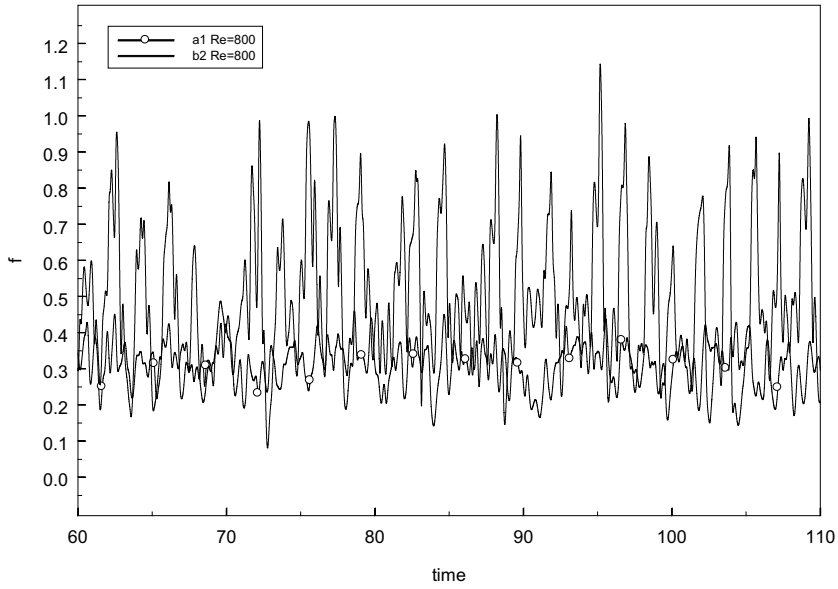

Fig. 6. Friction factor for a_1 and b_2 with $Re = 800$ as function of time.

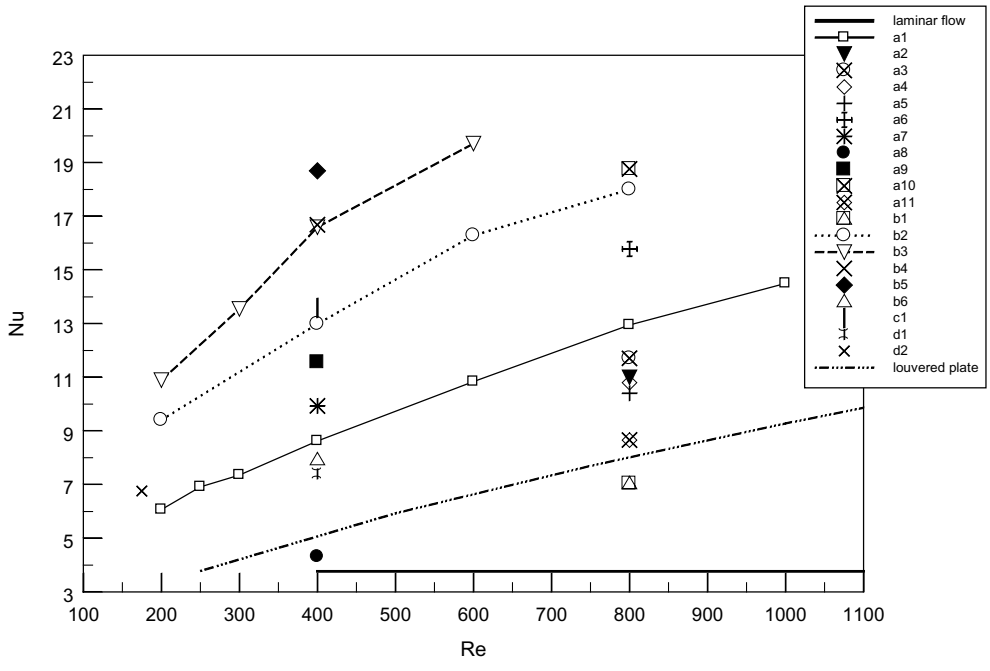

Fig. 7. Mean Nusselt number for different cases as function of channel Reynolds number.

with the best performance are b_5, b_3, b_4, b_2, a_{10} and c_1. The channel with baffles d_2 and the channel with two square bars a_9 and a_6 have the same performance. We can estimate from Fig. 9 the variation of Nu with fRe^3 for the rest of the cases based on the dependence of a_1, b_2 and b_3. Finally, comparisons of Nu for the same pumping power show heat transfer enhancement factors larger than 3.5 for the best results.

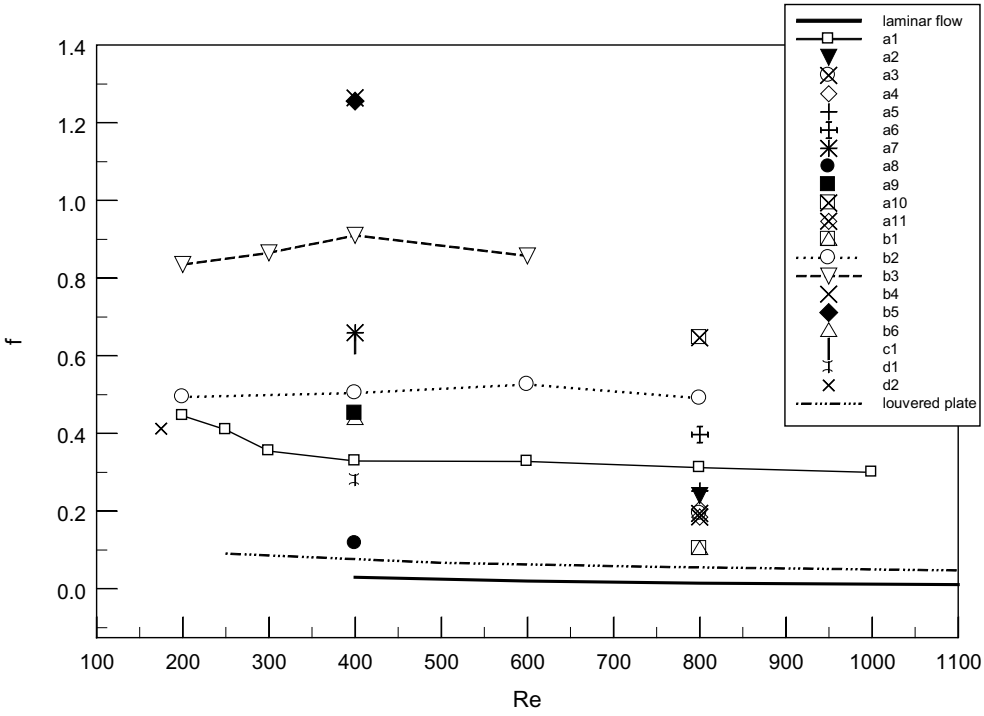

Fig. 8. Friction factor for different cases as function of channel Reynolds number.

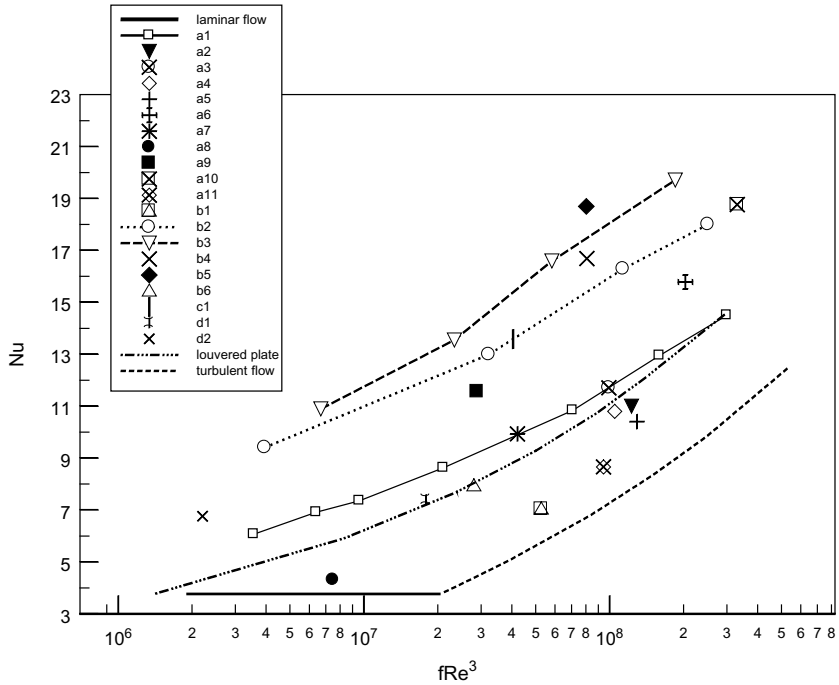

Fig. 9. Mean Nusselt number as function of pumping power for different cases. Data for louvered channel (3/16–11.1) from [17], data for laminar and turbulent flow in a plane channel from [16].

6. Conclusions

Two-dimensional Navier–Stokes simulations of heat and momentum transport in a plane channel with spatially periodic transverse vortex generators in the form of two square bars, one rectangular bar, or baffles were performed using the finite volume technique for the Reynolds number range $175 \leqslant Re \leqslant 1000$. Flows with simple, unsteady laminar behavior with only one frequency present, and others with complex, unsteady flow of transitional character were found depending on the Reynolds number and geometry. The best result with two square bars has a heat transfer enhancement of 5 and pressure drop increase of 43 for $Re = 800$. The arrangements with only one built-in rectangular bar had in general a better performance than the other configurations. The performance of all the configurations was very sensitive to the geometrical parameters, in particular to the choice of pitch.

Acknowledgement

Financial support received from FONDECYT Chile under grant number 1010400 is gratefully acknowledged.

References

[1] R.L. Webb, Principles of Enhanced Heat Transfer, John Wiley & Sons, New York, 1994.
[2] M. Greiner, P.F. Fischer, H.M. Tufo, Two-dimensional simulations of enhanced heat transfer in an intermittently grooved channel, ASME J. Heat Transfer 124 (2002) 538–545.
[3] C.H. Amon, D. Majumdar, C.V. Herman, F. Mayinger, B.B. Mikić, D.P. Sekulic, Numerical and experimental studies of self-sustained oscillatory flows in communicating channels, Int. J. Heat Mass Transfer 35 (1992) 3115–3129.
[4] R. Romero-Méndez, M. Sen, K.T. Yang, R.L. McClain, Enhancement of heat transfer in an inviscid-flow thermal boundary layer due to a Rankine vortex, Int. J. Heat Mass Transfer 41 (1998) 3829–3840.
[5] M. Fiebig, Vortices and heat transfer, Z. Angew. Math. Mech. (ZAMM) 77 (1997) 3–18.
[6] E.P.L. Roberts, A numerical and experimental study of transition processes in an obstructed channel flow, J. Fluid Mech. 260 (1994) 185–209.
[7] G. Wang, K. Stone, S.P. Vanka, Unsteady heat transfer in baffled channels, ASME J. Heat Transfer 118 (1996) 585–591.
[8] H. Kozlu, B.B. Mikić, A.T. Patera, Minimum-dissipation heat removal by scale-matched flow destabilization, Int. J. Heat Mass Transfer 31 (1988) 2023–2032.
[9] A. Valencia, Heat transfer enhancement due to self-sustained oscillating transverse vortices in channels with periodically mounted rectangular bars, Int. J. Heat Mass Transfer 42 (1999) 2053–2062.
[10] A. Valencia, J.S. Martin, R. Gormaz, Numerical study of the unsteady flow and heat transfer in channels with periodically mounted square bars, Heat Mass Transfer 37 (2001) 265–270.
[11] G. Bosch, Experimentelle and theoretische Untersuchung der instationären Strömung um zylindrische Strukturen, Dissertation, Universität Karlsruhe, Germany, 1995.
[12] M. Breuer, J. Bernsdorf, T. Zeiser, F. Durst, Accurate computations of the laminar flow past a square cylinder based on two different methods: lattice-Boltzmann and finite-volume, Int. J. Heat Fluid Flow 21 (2000) 186–196.
[13] S.V. Patankar, C.H. Liu, E.M. Sparrow, Fully developed flow and heat transfer in ducts having streamwise-periodic variation of cross-sectional area, ASME J. Heat Transfer 99 (1977) 180–186.
[14] S.V. Patankar, Numerical Heat Transfer and Fluid Flow, Hemisphere, Washington, DC, 1980.
[15] J.P. Van Doormaal, G.D. Raithby, Enhancements of the SIMPLE method for predicting incompressible fluid flows, Numer. Heat Transfer 7 (1984) 147–163.
[16] A.F. Mills, Basic Heat and Mass Transfer, Prentice Hall, New York, 1999.
[17] W.M. Kays, A.L. London, Compact Heat Exchangers, third ed., Krieger, Melbourne, FL, 1988.